SCIENCE CHINA
Information Sciences

• RESEARCH PAPER •

August 2022, Vol. 65 182403:1–182403:7
https://doi.org/10.1007/s11432-022-3436-y

RGB WGM lasing woven in fiber braiding cavity

Kun GE, Zhiyang XU, Dan GUO*, Ben NIU, Jun RUAN, Libin CUI & Tianrui ZHAI*

College of Physics and Optoelectronics, Faculty of Science, Beijing University of Technology, Beijing 100124*, China*

Received 2 January 2022/Revised 12 February 2022/Accepted 22 February 2022/Published online 11 July 2022

Abstract It is critical to realize woven and wearable red-green-blue (RGB) whispering gallery mode (WGM) lasing that is tunable and flexible in the fiber braiding cavity. However, it is still a challenge to achieve tunable full-color lasing with the large color gamut by a facile approach. Here, we design the braiding cavity to realize RGB WGM lasing with high performance. The braiding cavity consists of three optical fibers coated with dye-doped polymer. Each fiber therein serves as a resonant cavity to support multiple lasing modes. There is no interference owing to the air gap between them; therefore, we can achieve full-color WGM lasing. The lasing emission in our fiber braiding cavity covers a color gamut of 86.7% larger than standard RGB space. Our work may provide a platform for potential applications in white laser and integrated optoelectronic devices.

Keywords RGB, whispering gallery mode (WGM) lasing, fiber braiding cavity, full-color gamut

Citation Ge K, Xu Z Y, Guo D, et al. RGB WGM lasing woven in fiber braiding cavity. Sci China Inf Sci, 2022, 65(8): 182403, https://doi.org/10.1007/s11432-022-3436-y

1 Introduction

The whispering gallery mode (WGM) microcavity with small mode volume and high quality (Q) factor [1–5] has emerged as a promising platform for novel physical properties and potential applications in ultrasensitive detection [6–11], microlasers [12–18], biochemical and biological sensing [19–22], single nanoparticles detecting [23], and ultrahigh-Q polymer lasing [24]. The small mode volume leads to the significant enhancement of light-matter interaction, and the high Q factor implies a long photon lifetime and lower optical loss in the resonant cavity [1–3]. Besides, the red-green-blue (RGB) lasing covering the visible spectra has attracted much attention owing to the potential applications [25–28], such as optical displays [29–31], white light sources [32–34], and full-color lasing [35, 36]. In the past years, a lot of active materials have been used to fabricate the lasers, such as colloidal quantum dots [37], meter halide perovskite [38], dyes, and organic semiconductor polymer [39, 40].

The fiber braiding structure has two potential functions in white sources for laser display devices and next-generation devices for wearable sensors. The RGB lasing structure can be fabricated by mixing three gain dyes. However, the reabsorption among different gain dyes will hinder the lasing in the microcavity. Therefore, this strategy may hinder the practical application. The flexible woven has important applications in the next-generation devices, such as wearable sensors, wearable energy storage textiles, and smart electronic textiles [41–44]. The fiber braiding structure may be a facile approach to achieving wearable smart textiles. The weaving of three dye-coated fibers into full-color lasing is hardly reported.

Here, an ingenious and facile approach is used to achieve RGB WGM lasing by designing the fiber braiding cavity. The resonant cavity consists of three optical fibers coated with the dye-doped polymer, and it is fabricated by brush-coating technology. Therein, each fiber serves as an excellent WGM resonant cavity to provide multiple lasing modes. The spectrum properties of WGM lasing woven are investigated with a lower excitation threshold of 19.1 $\mu J/cm^2$. The narrowest spectral linewidth is measured to be 0.045 nm, which implies a low optical loss in the fiber braiding cavity. Moreover, there is no interference

* Corresponding author (email: dguo@bjut.edu.cn, trzhai@bjut.edu.cn)

owing to the air gap exist. Therefore, the full-color WGM lasing can be achieved in the fiber braiding cavity when pumped by an ultraviolet pumping source. By successively designing three optical fibers coated with the dye-doped polymer, we obtain seven lasing emissions including blue (B), green (G) and red (R) lasing, dual-color lasing (G+B), (R+B), (R+G) and full-color lasing (R+G+B). The lasing emissions cover a color gamut 86.7% larger than the standard RGB (sRGB) space, showing great potential in compact white sources and laser display devices.

2 Experiments

2.1 Materials

The chemical reagents include light-emitting molecules Disodium 4, 4'-Bis (2-sulfonatostyryl)biphenyl (S420 D-36543 Tianjin Heowns Biochem LLC, Tianjin, China), Fluorescein sodium salt (uranin A46092 AI LAN (Shanghai) Chemical Technology Co., Ltd., Shanghai, China), Rhodamine B (RhB, Tianjin Fuchen Chemical Reagents Factory, Tianjin, China), and Polyvinyl alcohol (PVA) (S27039-500g, Beijing Hong Hu United Chemical Products Co., Ltd.) serving as a matrix.

2.2 Fabrication of fiber braiding cavity

The PVA solution is formed by dissolving PVA in deionized water with the concentration of 16 wt%, and S420, uranin are dissolved in deionized water with the concentration of 10 mg/mL and 9 mg/mL, and RhB is dissolved in ethanol with the concentration of 6 mg/mL to form three kinds of dye solution. Next, PVA solution is mixed with three kinds of dyes solution respectively, with the volume ratio of 1:1 under magnetic stirring for 30 min. Thus, three-color dyes doped polymer ink is formed, and they are brush coated onto the optical fiber to form red-emitting fiber (R-fiber), green-emitting fiber (G-fiber), and blue-emitting fiber (B-fiber). Further, the RGB WGM lasers are woven to form a fiber braiding cavity. The PVA acts as the matrix and adhesion agent to form the cavity to offer the WGM resonation. Figure 1(a) shows the design scheme of the fiber braiding cavity. The normalized absorption and photoluminescence (PL) spectrum for three active materials can be found in Figure S1.

The frame consists of commercial optical fiber and fluorescent cladding. The fiber is made of the fiber core, cladding, and coating. The diameter of fiber core and cladding are 9 and 125 μm, respectively. The refractive index of fiber core and cladding are 1.444 and 1.427, respectively. The fiber coating is removed in the experiment. Therefore, the thickness of fiber is 125 μm. The dye-doped polymer layer's thickness is about 30 μm (in Figure S2). The effective refractive index of microcavity is 1.55. The individual dye-coated fiber can serve as an excellent microscale WGM resonant cavity to support the multiplemode lasing. Moreover, there is no interference owing to the air gap existing in the fiber braiding cavity. Therefore we can obtain the RGB WGM lasing when pumped by ultraviolet light, simultaneously. Figure 1(b) presents the image of the fiber braiding cavity, which indicates the three fibers can be integrated to form the fiber braiding cavity and the air gap exists between them. The PL spectrum for RGB lasing at the center wavelength of $\lambda_1 = 443$ nm, $\lambda_2 = 563$ nm, and $\lambda_3 = 628$ nm, for B-fiber, G-fiber, and R-fiber, respectively (in Figure 1(c)). Moreover, the full-color WGM lasing can be achieved when woven lasing is excited by the single pump source in the fiber braiding cavity.

3 Results and discussion

Therein, the dye-coated fiber is smooth so that it can serve as WGM resonant cavity to support optical feedback and oscillation. Therefore, each fiber acts as an excellent gain cavity to provide multiple lasing modes. To identify the fiber braiding cavity performance of RGB WGM lasing, the fiber is excited with a μ-PL operating system (FST2-MPL-400L1) under a nanosecond laser with the wavelength of 343 nm (third harmonics from a 1030 nm Yb:YAG laser, repetition frequency of 200 Hz, and pulse width of 1 ns). The laser beam is adjusted to fully cover the whole sample.

The spectrum characterization of three individual optical fibers coated with dye-doped polymer is investigated. Figures 2(a)–(c) provide the emission spectra of three dye-coated fibers with pumping power density increasing from 4.5 to 52.3 μJ/cm^2, 31.7 to 141 μJ/cm^2, and 4.5 to 82.9 μJ/cm^2, for B-fiber, G-fiber, and R-fiber, respectively. The results indicate that the dye-coated fibers can serve as WGM resonant cavity, with strong mode confinement in the dye-coated fiber (in Figure S3). Taking the R-fiber

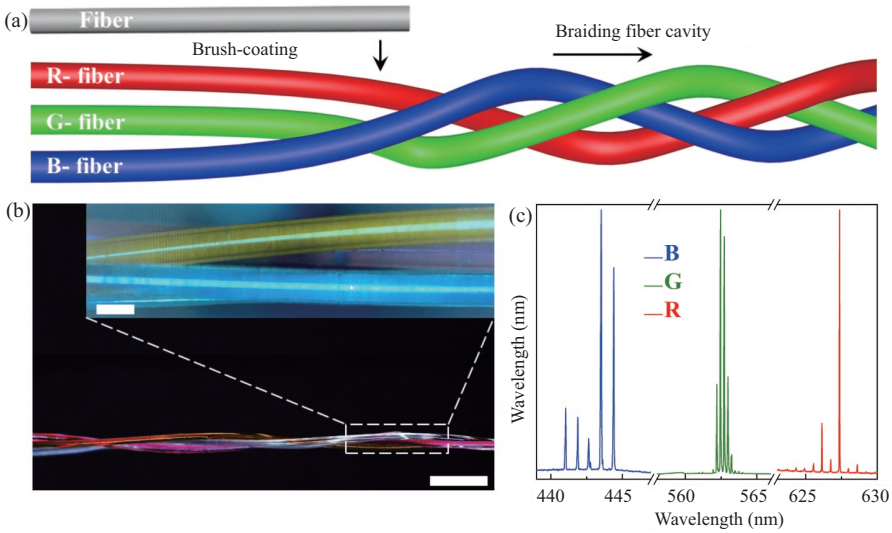

Figure 1 (Color online) Fabrication scheme for RGB WGM laser woven into a fiber braiding cavity. (a) Schematic illustration of the fabrication progress of RGB lasing braiding cavity; (b) far-filed picture (scale bar: 500 μm) and high-magnification picture (scale bar: 150 μm) for the RGB braiding cavity; (c) the PL spectra of RGB emission.

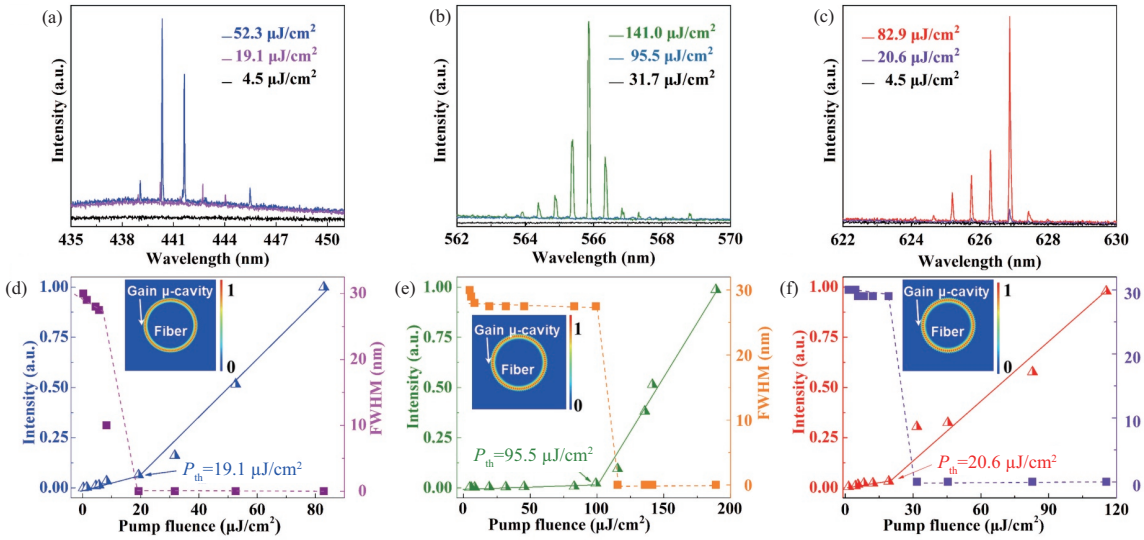

Figure 2 (Color online) The RGB WGM lasing. (a)–(c) The spectra of RGB lasing with different pump power densities. (d)–(f) The relationship between peak intensity, FWHM, and pump fluence at the wavelength of 440.3, 565.8, and 626.9 nm, for B-fiber, G-fiber, and R-fiber, respectively. The top-left illustration is the simulated distribution of electric field intensity in the transverse cross-section, respectively.

as an example, the uniform spontaneous emission is observed from the entire R-fiber at low pumping fluence. The bright red emission begins to be observed on the circumference edge of the R-fiber at the pump fluence of 20.6 μJ/cm^2. Then, several equidistant discrete narrow peaks wavelengths are clearly observed when the pump power density exceeds 20.6 μJ/cm^2, indicating the strong mode confinement and the lasing forming (in Figure S4). The narrow peaks wavelength corresponds to the WGM mode selectively amplified by the resonant cavity, and it is revealed by the bright circumference edge in the fiber (in Figure S4).

Figures 2(d)–(f) show the relationship between peak intensity (solid line) and pump power density at the wavelength of 440.3, 565.8 and 626.9 nm, for the B-fiber, G-fiber and R-fiber, respectively. The lasing threshold is about 19.1, 95.5 and 20.6 μJ/cm^2, respectively. The dye-coated fiber can act as a resonant cavity to support the stimulated radiation amplification, so that it can reduce the WGM lasing threshold. The relationship between full width at half maximum (FWHM) (dashed line) and pump power density is shown in Figures 2(d)–(f). We simulate the electric field intensity distribution in the

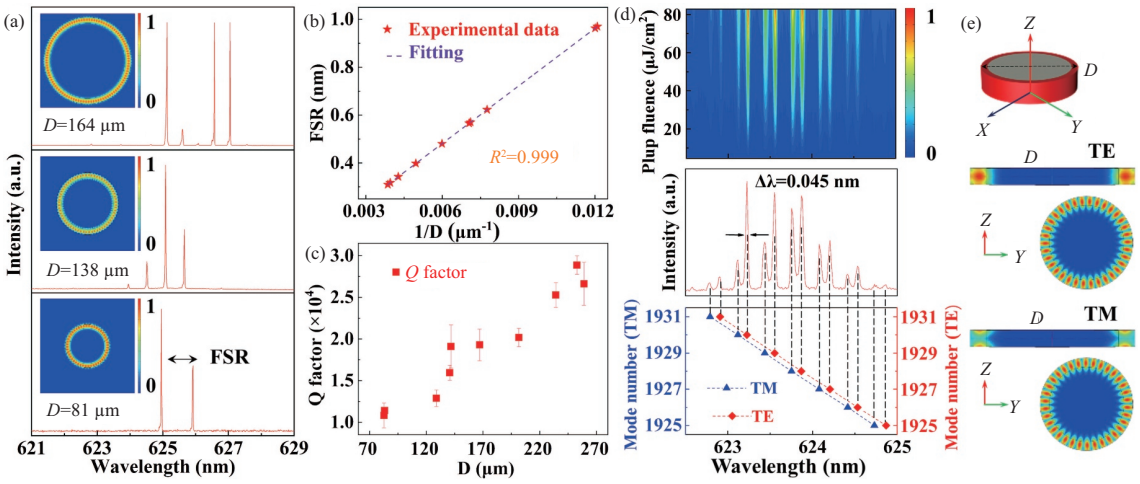

Figure 3 (Color online) The PL spectra corresponding to different cavity diameters. (a) The multiple mode lasing spectra from individual fiber cavity with diameters of 164, 138, and 83 μm from top to bottom. The top-left inset is the electric field distribution; (b) the calculated FSR corresponding to $1/D$, showing the linear correlation, the purple dashed line is fitted well with (1); (c) the relationship between Q factor and D; (d) spectral map of the emission intensity with pump fluence (top), and the relationship between mode numbers and peak wavelength determined by (2); (e) schematic diagram of the experimental setup and the distribution of electric field intensity for TE and TM mode.

transverse cross-section using the commercial software COMSOL multi-physics 5.4 (top-left illustration in Figures 2(d)–(f)). The lasing modes distribution cannot be distinguished if it is simulated according to the actual size of the fiber resonant cavity. According to the scaling law, the size of numerical simulation can be reduced dozens of times. The strong mode confinement excites in circumference edge of the dye-coated fiber. The numerically simulated and experimental results are in good agreement.

We have investigated the relationship between free spectral range (FSR) and Q factor by altering the size of the dye-coated fiber resonant cavity. Figure 3(a) provides the PL emission spectra for red-emitting lasers with three typical diameters, and the FSR is 0.48, 0.57, and 0.97 nm, corresponding to the diameter of 164, 138 and 81 μm (from top to bottom), respectively, recorded by a spectrometer with a resolution of 0.001 nm. The mode spacing decreases with the diameter of the resonant cavity, which can be readily tuned by readily tailoring the fiber diameters. The high-order mode and low-order mode spacing is different in the same resonant cavity owing to the superposition of two different lasing mode sets (in Figure S5). For resonant cavities with different diameters, the path of the optic limitation region is greatly increased with the increasing of the diameter of the resonant cavity. The corresponding numerical simulation of electric field distribution in the transverse cross-section demonstrates the WGM lasing behaviors (below left in Figure 3(a)). The lasing modes are confined into the dye-coated fiber, which is in good agreement with the experimental phenomena.

The dye-coated fiber resonant cavity can support optical feedback and oscillations due to total internal reflection between the gain cavity and air. According to the WGM equation:

$$\mathrm{FSR} = \frac{\lambda^2}{\pi n_{\mathrm{eff}} D}, \tag{1}$$

where λ is the center wavelength, n_{eff} is the effective refractive index, and D is the dye-coated fiber diameter, respectively. The dye-coated fiber resonant cavity is investigated by measuring different PL spectra with the altered diameter of the dye-coated fiber. Figure 3(b) shows the relationship between FSR and D. The red stars are the experimental data of different FSR for the lasing fibers with altered diameters. The purple dashed line is well fitted with (1), with the slope as a constant, indicating the n_{eff} is a definite value when λ is changeless and π is constant in the experiment. The red squares show the relationship between the calculated Q factor and various diameters in the experiment as shown in Figure 3(c). The Q value is calculated using the equation $Q \approx \lambda/\Delta\lambda$, where λ is the center wavelength and $\Delta\lambda$ is the linewidth of the peak wavelength. The calculation of Q value is from 1×10^4 to 3×10^4 when altering dye-coated fiber diameter from 80 to 265 μm.

The spectral map of the normalized emission intensity with different pump power densities is shown (top in Figure 3(d)). The lasing peak wavelength is almost changeless with increasing the pump fluence, which demonstrates the WGM lasing is stable.

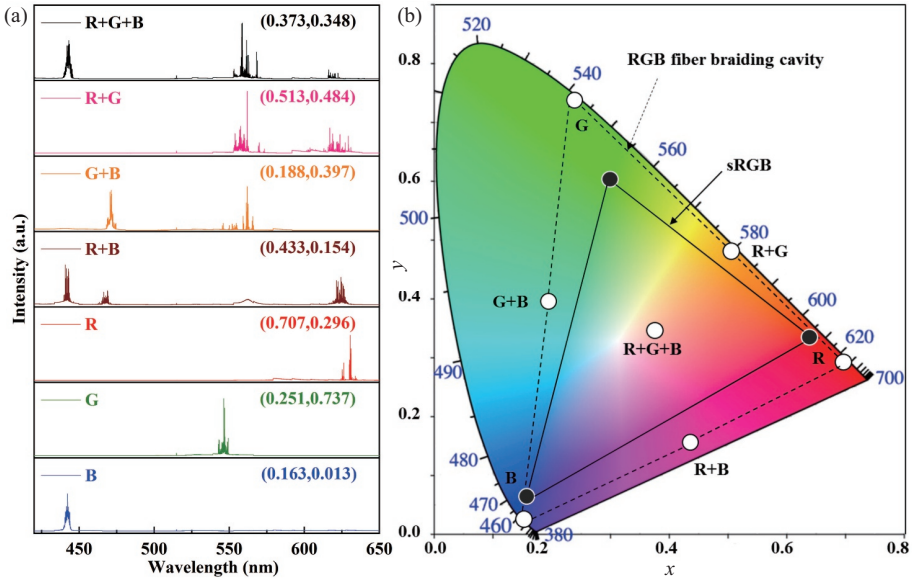

Figure 4 (Color online) Full-color lasing in the fiber braiding cavity. (a) PL spectra for seven combinations of R, G, and B lasing fibers. In the top-right illustration, the numbers show the CIE1931 coordinates calculated from the corresponding spectra. From bottom to top: B-, G-, R-, G+B-, R+B-, R+G- and R+G+B-emitting lasing fibers. (b) Chromaticity diagram of lasing peaks (a) with white circles. The dashed and solid lines show the range of the achievable color gamut for the RGB fiber braiding cavity and sRGB space, respectively.

The peak wavelength can be determined by the WGM equation:

$$m\lambda_m = \pi n_{\text{eff}} D, \tag{2}$$

where angular quantum number m is a positive integer, and λ_m is the peak wavelength. The relationship between peak wavelength and mode numbers is shown in Figure 3(d). The theoretical calculation demonstrates the lasing peaks belong to first-order transverse magnetic (TM) and transverse electric (TE) modes, and the corresponding mode numbers are from 1925 to 1931. The red squares and blue triangles provide the relationship between peak wavelength TE modes and TM modes, respectively. Then, we investigate the distribution of electric field intensity with TE and TM modes, and Figure 3(e) presents the physical model. The numerically simulated results show that TE modes' output intensity is higher than TM modes, which is consistent with the experiment. Microlasers with linear polarization have excellent practical applications. To study the polarization of the dye-coated fiber, the emission spectrum as a function of polarizer angle (θ) is recorded as shown in Figure S6.

Here, the full-color expression was recorded through the emission spectra in a fiber braiding cavity. The blue-color lasing is observed when the excitation beam is focused on the B-fiber resonant cavity, lasing wavelength at 443 nm. As the excitation beam is manipulated to excite on the G-fiber (or R-fiber), we can obtain the green-color (or red-color) lasing, lasing wavelength at 545 and 628 nm, respectively. The B-fiber has two PL emission peaks (in Figure S1); therefore, we may obtain different PL lasing spectrums. The dual-color lasing (R+B, G+B, and R+G) can be achieved when the R-fiber and B-fiber, the G-fiber and B-fiber, and the R-fiber and G-fiber are simultaneously pumped above their thresholds. The full-color lasing is realized in the fiber braiding cavity when the woven cavity is pumped, simultaneously (in Figure 4(a)). The numbers show the CIE1931 coordinates calculated from the corresponding spectra (top right in Figure 4(a)). The corresponding optical images with B-, G-, R-, G+B-, R+B-, R+G-, and R+G+B-emitting fibers are shown in Figure S7. The chromaticity diagram based on the International Commission on Illumination (CIE) 1931 color diagram is shown in Figure 4(b). The white circles are from different combination of lasing spectra in Figure 4(a) and the lasing emission in the fiber braiding cavity covers a color gamut 86.7% larger than the standard RGB space (in Table S1). The white circle named "R+G+B" denotes the CIE value of the mixed white light. Therefore, the full-color WGM woven lasing device is realized in a fiber braiding cavity. It may provide a platform for potential applications in integrated optoelectronic devices and white light sources.

4 Conclusion

In summary, we realize the RGB WGM lasing with the low threshold and high Q factor by designing a fiber braiding cavity. Each dye-coated fiber can serve as a WGM resonant cavity to provide multiplemode lasing, and full-color WGM lasing is achieved by a braiding fiber cavity. Moreover, our laser emissions cover a color gamut 86.7% larger than the standard RGB space in the fiber braiding cavity. This work may provide a platform for potential applications in wearable and integrated optoelectronic devices.

Acknowledgements This work was supported by Beijing Natural Science Foundation (Grant No. Z180015) and National Natural Science Foundation of China (Grant No. 61822501).

Supporting information Figures S1–S7, Table S1. The supporting information is available online at info.scichina.com and link.springer.com. The supporting materials are published as submitted, without typesetting or editing. The responsibility for scientific accuracy and content remains entirely with the authors.

References

1 Vahala K J. Optical microcavities. Nature, 2003, 424: 839–846
2 Armani D K, Kippenberg T J, Spillane S M, et al. Ultra-high-Q toroid microcavity on a chip. Nature, 2003, 421: 925–928
3 McCall S L, Levi A F J, Slusher R E, et al. Whispering-gallery mode microdisk lasers. Appl Phys Lett, 1992, 60: 289–291
4 Vernooy D W, Ilchenko V S, Mabuchi H, et al. High-Q measurements of fused-silica microspheres in the near infrared. Opt Lett, 1998, 23: 247–249
5 Zhizhchenko A, Syubaev S, Berestennikov A, et al. Single-mode lasing from imprinted halide-perovskite microdisks. ACS Nano, 2019, 13: 4140–4147
6 Heylman K D, Thakkar N, Horak E H, et al. Optical microresonators as single-particle absorption spectrometers. Nat Photon, 2016, 10: 788–795
7 Zhang Y N, Zhou T, Han B, et al. Optical bio-chemical sensors based on whispering gallery mode resonators. Nanoscale, 2018, 10: 13832–13856
8 Vollmer F, Arnold S. Whispering-gallery-mode biosensing: label-free detection down to single molecules. Nat Methods, 2008, 5: 591–596
9 Vollmer F, Braun D, Libchaber A, et al. Protein detection by optical shift of a resonant microcavity. Appl Phys Lett, 2002, 80: 4057–4059
10 Dantham V R, Holler S, Barbre C, et al. Label-free detection of single protein using a nanoplasmonic-photonic hybrid microcavity. Nano Lett, 2013, 13: 3347–3351
11 Zhi Y, Yu X C, Gong Q, et al. Single nanoparticle detection using optical microcavities. Adv Mater, 2017, 29: 1604920
12 Frolov S V, Shkunov M, Vardeny Z V, et al. Ring microlasers from conducting polymers. Phys Rev B, 1997, 56: 4363–4366
13 Xu Z, Zhai T, Shi X, et al. Multifunctional sensing based on an ultrathin transferrable microring laser. ACS Appl Mater Interfaces, 2021, 13: 19324–19331
14 Ta V D, Chen R, Sun H D. Tuning whispering gallery mode lasing from self-assembled polymer droplets. Sci Rep, 2013, 3: 1362
15 Xu Z, Tong J, Shi X, et al. Tailoring whispering gallery lasing and random lasing in a compound cavity. Polymers, 2020, 12: 656
16 Chiasera A, Dumeige Y, Féron P, et al. Spherical whispering-gallery-mode microresonators. Laser Photon Rev, 2010, 4: 457–482
17 Wei G Q, Wang X D, Liao L S. Recent advances in organic whispering-gallery mode lasers. Laser Photonics Rev, 2020, 14: 2000257
18 Wei C, Gao M, Hu F, et al. Excimer emission in self-assembled organic spherical microstructures: an effective approach to wavelength switchable microlasers. Adv Opt Mater, 2016, 4: 1009–1014
19 Gao M, Wei C, Lin X, et al. Controlled assembly of organic whispering-gallery-mode microlasers as highly sensitive chemical vapor sensors. Chem Commun, 2017, 53: 3102–3105
20 Wang Y, Zeng S, Humbert G, et al. Microfluidic whispering gallery mode optical sensors for biological applications. Laser Photonics Rev, 2020, 14: 2000135
21 Pasquardini L, Berneschi S, Barucci A, et al. Whispering gallery mode aptasensors for detection of blood proteins. J Biophoton, 2013, 6: 178–187
22 Squires T M, Messinger R J, Manalis S R. Making it stick: convection, reaction and diffusion in surface-based biosensors. Nat Biotechnol, 2008, 26: 417–426
23 Zhu J, Ozdemir S K, Xiao Y F, et al. On-chip single nanoparticle detection and sizing by mode splitting in an ultrahigh-Q microresonator. Nat Photon, 2010, 4: 46–49
24 Tang S J, Liu Z, Qian Y J, et al. A tunable optofluidic microlaser in a photostable conjugated polymer. Adv Mater, 2018, 30: 1804556
25 Fu Y, Zhai T. Distributed feedback organic lasing in photonic crystals. Front Optoelectron, 2020, 13: 18–34
26 Kong Y, Dai H, He X, et al. Reconfigurable RGB dye lasers based on the laminar flow control in an optofluidic chip. Opt Lett, 2018, 43: 4461–4464
27 Zhu M, Duan Y, Liu N, et al. Electrohydrodynamically printed high-resolution full-color hybrid perovskites. Adv Funct Mater, 2019, 29: 1903294
28 Dang C, Lee J, Breen C, et al. Red, green and blue lasing enabled by single-exciton gain in colloidal quantum dot films. Nat Nanotech, 2012, 7: 335–339
29 Zhang W, Zhang Y M, Xie F, et al. A single-pixel RGB device in a colorful alphanumeric electrofluorochromic display. Adv Mater, 2020, 32: 2003121
30 Müller C D, Falcou A, Reckefuss N, et al. Multi-colour organic light-emitting displays by solution processing. Nature, 2003, 421: 829–833
31 Kim T H, Cho K S, Lee E K, et al. Full-colour quantum dot displays fabricated by transfer printing. Nat Photon, 2011, 5: 176–182

32 Zhao Y S, Fu H, Hu F, et al. Tunable emission from binary organic one-dimensional nanomaterials: an alternative approach to white-light emission. Adv Mater, 2008, 20: NA
33 Li S, Wang L, Zhai T, et al. Red-green-blue plasmonic random lasing from cascaded polymer slices. Laser Phys Lett, 2018, 15: 085803
34 Foucher C, Guilhabert B, Kanibolotsky A L, et al. RGB and white-emitting organic lasers on flexible glass. Opt Express, 2016, 24: 2273–2280
35 Ge K, Shi X, Xu Z, et al. Full-color WGM lasing in nested microcavities. Nanoscale, 2021, 13: 10792–10797
36 Zhao J, Yan Y, Gao Z, et al. Full-color laser displays based on organic printed microlaser arrays. Nat Commun, 2019, 10: 870
37 Hayat A, Tong J H, Chen C, et al. Multi-wavelength colloidal quantum dot lasers in distributed feedback cavities. Sci China Inf Sci, 2020, 63: 182401
38 Zhang X, Yan S, Tong J, et al. Perovskite random lasers on fiber facet. Nanophotonics, 2020, 9: 935–941
39 Tong J H, Shi X Y, Wang Y, et al. Flexible plasmonic random laser for wearable humidity sensing. Sci China Inf Sci, 2021, 64: 222401
40 Duong Ta V, Chen R, Ma L, et al. Whispering gallery mode microlasers and refractive index sensing based on single polymer fiber. Laser Photonics Rev, 2013, 7: 133–139
41 Yetisen A K, Qu H, Manbachi A, et al. Nanotechnology in textiles. ACS Nano, 2016, 10: 3042–3068
42 Qi K, Zhou Y, Ou K, et al. Weavable and stretchable piezoresistive carbon nanotubes-embedded nanofiber sensing yarns for highly sensitive and multimodal wearable textile sensor. Carbon, 2020, 170: 464–476
43 Huang Y, Hu H, Huang Y, et al. From industrially weavable and knittable highly conductive yarns to large wearable energy storage textiles. ACS Nano, 2015, 9: 4766–4775
44 Weng W, Chen P, He S, et al. Smart electronic textiles. Angew Chem Int Ed, 2016, 55: 6140–6169